Published by :
http://www.ijert.org

International Journal of Engineering Research & Technology (IJERT)
ISSN: 2278-0181
Vol. 5 Issue 10, October-2016

Ammonia Gas Sensing Performance of Polyaniline-SnO_2

Janhavi Talegaonkar[a],
Dept. of Physics,
Smt. P. K. Kotecha Mahila Mahavidyalala, Bhusawal
District – Jalgaon (MHS), India, 425201

D. R. Patil
Bulk and Nanomaterials Research Laboratory,
Dept. of Physics, R. L. College, Parola
District – Jalgaon (MHS), India, 425111

***Abstract*- Nanocomposite samples of polyaniline-SrO_2 were prepared by loading pure polyaniline (PANI) by post-transition metal oxide (SnO_2) as an additive. Nanocomposites of PANI-SnO_2 were prepared with three different molar concentrations of SnO_2 using in situ oxidative polymerization of aniline in presence of SnO_2. UV-Visible spectroscopy of prepared samples of PANI-SnO_2 revealed emraldine salt phase of polyaniline. XRD patterns reflect the nano crystallite size of PANI-SnO_2 composite. Transmission electron microscopic study confirms the nano-sized of prepared composite samples. Scanning Electron Microscopy of nanocomposite showed change in surface morphology with the variation in concentration of SnO_2. PANI-SnO_2 (0.25 M) nanocomposite exhibit a response to CO_2 at quit higher temperature. The effects of surface microstructure with variation in SnO_2 concentrations and surface activation with CuO on the sensor response, selectivity, recovery and long term durability of the sensor in the presence of NH_3 and other gases were studied and discussed. SnO_2 loaded PANI is outstanding in promoting the NH_3 gas sensing performance of the material. CuO as an activator in PANI-SnO_2 enhances ammonia sensing performance of the prepared sensor samples at room temperature.**

Keywords— Polyaniline, SnO_2, Nanocomposite, Ammonia gas Sensor, Room temperature.

I. INTRODUCTION

In everyday life, gas sensors have a broad range of increasing applications regarding environmental monitoring and protection, clinical and health care, food processing, industrial development, etc. Semiconducting metal oxides have been studied extensively for sensing different gases. In particular SnO_2 [1], ZnO [2-7], Ferrites [8], $LaAlO_3$ [9], Cu_2S [10], etc. are studied extensively. However, there are some significant disadvantages of metal oxide gas sensors such as high operating temperature, lack of selectivity and sensitivity at ambient temperature, instability over long period, etc. Recent developments in the field of conducting polymer promise future progress in certain areas of modern technology such as microelectronics, sensors, biosensors or chemical and biochemical engineering [11-13]. Gas sensors are important for monitoring environmental quality and safety. Hazardous gases, like liquefied petroleum gas (LPG), have been widely used for several industrial and domestic applications. The development of gas sensors is imperative due to the concern of safety requirements, particularly for detection of LPG. Gas sensing devices based on inorganic materials, generally have low selectivity to specific target gases and operating temperature [14-16] thus suffering with high power consumption, reduced sensor life, limited portability, etc. In order to overcome these problems recently, conducting polymers found suitable as a gas sensor. Recent studies showed that, conducting polymers are sensitive to wide range of gases and vapors [17-18, 22-26].

However, the problems with the conducting polymers are their low processability, their mechanical strength [19-21], poor chemical stability, etc. Out of various conducting polymers, Polyaniline (PANI) is most studied for its various applications. Gas sensors based on PANI show major disadvantage of poor selectivity for particular gas against other gases. Because conducting PANI can be doped and undoped by redox reactions and their doping level get altered by transferring electrons from the gases or to the gases. Electron acceptor (oxidizing) gases such as NO_2, Cl_2 etc. remove electrons from the aromatic ring of PANI which shows enhanced doping level and electrical conductivity of PANI. An opposite process takes place when electron donating (reducing) gases such as NH_3, H_2S, C_2H_5OH, etc. react with active layer of PANI. It is a major challenge to improve selectivity and stability in case of gas sensors based on PANI. As an option, composition of organic and inorganic materials, PANI and metal particles, provides enhancement of sensor characteristics such as selectivity, sensitivity, etc. and mechanical strength. Recently researchers are working with many of such composition like PANI-SnO_2 as ammonia sensor [22] PANI-ZnO [23] and PANI- CdS thin films as LPG sensor [24]. PANI-WO_3 thick films showed remarkable response to LPG [25]. PANI-Cu pellets were fabricated for chloroform vapor sensing [26].

In the present work, efforts are taken to develop the ammonia sensor by modifying PANI and its compositions with SnO_2, which could be able to detect various gases at trace level (ppm, ppb or even sub-ppb level).

II. EXPERIMENTAL DETAILS

All reagents $Sncl_2$, ethanol, liquid ammonia, Nitric acid, Aniline, Ammonium per sulphate were purchased from sigma. All chemicals were of analytical grade and used as received.

II. (A) SYNTHESIS OF MATERIALS

Nanostructured SnO_2 is synthesized by disc type Ultra sonicated microwave assisted centrifuge technique. Initially, 1M solution of $SnCl_2$ was prepared in double distilled water, 2-3 ml ethanol was added and solution was stirred rigorously using magnetic stirrer. Liquid ammonia was then added in it very slowly, drop by drop, to maintain the pH of the solution up to 8.3 to 10. White precipitate obtained was collected and washed. This precipitate was then provided ultrasonic treatment for 6 hrs. followed by calcinations at 500^0C for 5 hrs. and finally, we get white powder of nanoscale SnO_2.

Composite samples of PANI-SnO_2 were prepared with three different molar concentrations of SnO_2 using in situ oxidative polymerization of aniline in presence of SnO_2. Aniline (0.5M) was added to the solution of 1M HNO_3. In this

International Journal of Engineering Research & Technology (IJERT)
ISSN: 2278-0181
Vol. 5 Issue 10, October-2016

solution, initially prepared SnO_2 was added with various molar concentrations (0.5M, 0.25M, and 0.125M) for various composite samples of PANI-SnO_2. The solution was stirred continuously using magnetic stirrer. (0.1M) ammonium per sulphate was added. After 4 to 5 hrs. solution was turn to dark green color, which is an indication of oxidation of aniline. The solution was then allowed to stir for 24 hrs. Green color ppt obtained, was filtered, washed and dried at 80^0C for 2 hrs. The dark green powder samples of PANI-SnO_2 were obtained. These dry powder samples were transformed in to thick films using screen printing technique, as explained earlier in chapter 2. Fabricated thick films were fired at 100^0C.

II. (B) CHARACTERIZATION

These prepared samples were characterized by using X-ray diffraction measurements, with Rigaku diffractometer using CuKu (λ= 1.542 nm) radiation over 2θ range from 20^0 to 80^0, UV-Visible spectroscopy using 300 to 1100 nm wave length, FTIR over 400 to 4000 cm^{-1}, was studied. The microscopy and micro-evaluations were performed with scanning electron microscopy technique (SEM& EDAX) and transmission electron microscopy. The electrical behavior and gas sensing performance of samples was checked.

III. RESULTS AND DISCUSSION

III (A) UV-VISIBLE SPECTROSCOPIC STUDIES

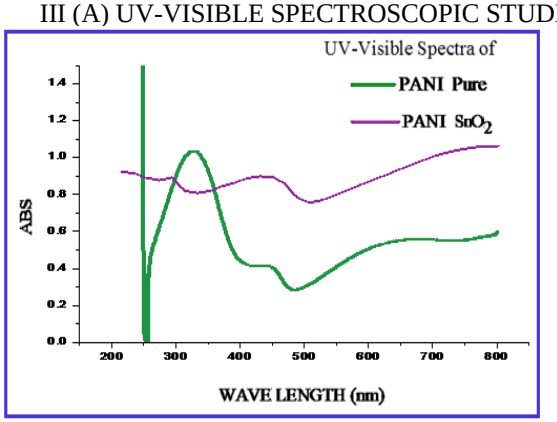

Fig. 1: UV-Visible spectroscopy of PANI-SnO_2

Fig. 1 depicts the UV-Visible spectra of pure PANI and PANI-SnO_2 (0.25M) composite sample. Fig. 1 distinctly reveals broad band of pure PANI at 325 nm, which is attributed to π - π transition of Benznoid ring. This peak is followed by a shoulder rise at 450 nm indicating formation of positive radical cation during oxidation of monomer. Broad peaks of pure PANI at 650 nm, associated to π - polaron transition due to inter ring charge transfer due to excitation of Benznoid ring to Quinoid ring. It depends on oxidation state of PANI. UV absorption spectra of PANI- SnO_2 show π - π^* transition of Benznoid ring at 280 nm. A peak at 420 nm exhibits polaron-π^* transition. The peak at 800 nm is attributed to π-polaron transition. The characteristic peak of π - π^* and π-polaron transition at 280 nm and 800 nm respectively attributed to the doping level and formation of polaron. As compared with pure PANI, optical spectra of PANI-SnO_2 shows shift towards lower wavelength. In addition, it is observed the increased level of absorption for PANI-SnO_2 composite. This is characteristic property of oxide. This proves the incorporation of SnO_2 in PANI matrix. It confirms formation of PANI-SnO_2 nanocomposites.

III (B) FTIR SPECTROSCOPIC STUDIES

FTIR spectrum of pure PANI is explained in Fig. 5 (a) of chapter 2. Fig. 2 shows FTIR spectrum of PANI-SnO_2 nanocomposite, shows characteristics peak at ~2923 cm^{-1} attributed to N-H stretching mode suggesting presence of N-H groups in aniline unit. The band at ~1599 cm^{-1} is attributed to stretching vibrations in quinoid N=Q=N ring. The band at ~1448 cm^{-1} is attributed to stretching vibrations in Benznoid N=B=N ring. The band at 1299 cm^{-1} is attributed to plane bending of C-H, formed during protonation. Peaks at 805 cm^{-1} reveal the presence of SnO_2 particles exhibiting the shift of characteristic frequencies towards the lower side. In FTIR spectra of pure PANI and composite of PANI-SnO_2, similar bands are observed over the range 400 - 4000 cm^{-1}. This indicates that the main constituents of PANI and PANI-SnO_2 composite have same chemical structures. However, shift of characteristic peaks is observed in PANI-SnO_2 composite sample. Such a shift may be described due to the formation of hydrogen bonding between tin oxide and NH group of PANI on the surface of tin oxide [27].

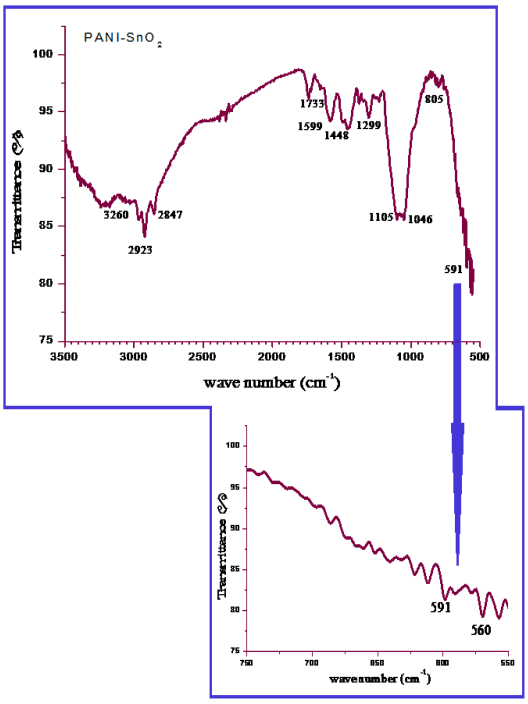

Fig. 2: FTIR spectrograph of PANI-SnO_2

III (C) X-Ray diffraction study

Fig. 3 shows X-Ray diffraction graph of PANI, PANI-SnO_2 and CuO activated PANI-SnO_2. The XRD measurements were performed with BRUKER AXSD 8 (Germany) advance model X ray diffraction with CuKα_1 (λ=1.54056A^0) radiation in the 2θ range 20^0- 80^0. The XRD pattern of pure PANI, in Fig. 3 (a) indicates the prominent broad diffraction peak at 23.98^0, suggesting the amorphous nature of PANI along with

International Journal of Engineering Research & Technology (IJERT)
ISSN: 2278-0181
Vol. 5 Issue 10, October-2016

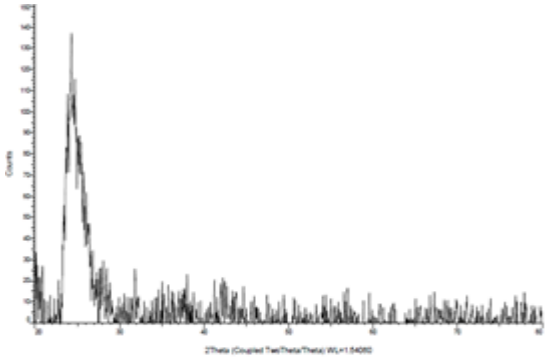

Fig. 3 (a) XRD pattern of pure PANI

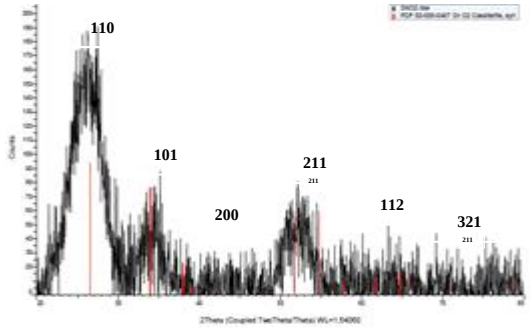

Fig. 3 (b): XRD pattern of PANI-SnO_2

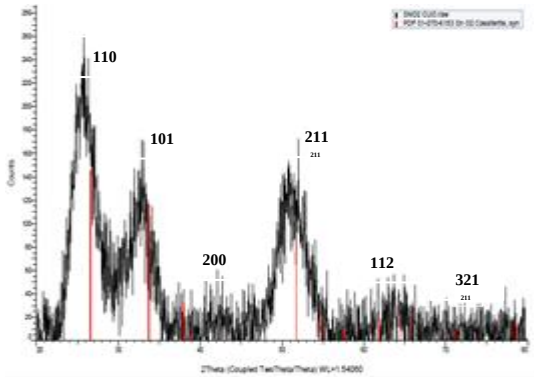

Fig. 3 (c): XRD pattern of CuO activated PANI-SnO_2

55.4% crystallinity due to synthesis in strong acidic aqueous medium (1M HNO_3).

Fig. 3 (b and c) indicate XRD peaks of PANI-SnO_2 and CuO activated PANI-SnO_2, showing prominent peaks attributed to (110), (101), (200) and (211) planes at 26.57^0, 33.8^0, 37.95^0 and 51.75^0 respectively, which is attributed to typical tetragonal structure (JCPDS DATA CARD 41-1445). For tetragonal structure, lattice constants a = b, a and c are determined by using the formula:

$$\frac{1}{d^2} = \frac{h^2 + k^2}{a^2} + \frac{l^2}{c^2}$$

The average value of lattice parameters was found to be a=b=4.74A^0 and c=3.186 A^0. While standard bulk value for tin oxide crystalline structure is a=b=4.738 A^0 and c=3.187 A^0. This suggests that SnO_2 grains in the thick film are strained may be due to the average physical size of the grain themselves [28]. Average crystallite size was estimated by using Scherer's formula:

$$d = \frac{k\lambda}{\beta \cos\theta}$$

Where d is the crystallite size, k is 0.9, wavelength of X ray radiation λ= 1.542 A^0 and θ is angle of diffraction. The crystallite size of PANI-SnO_2 nanocomposite is found to be ~ 6.8 nm. Fig. 3 (a-c) reveals the preferred orientation for SnO_2 is along the plane (110) [29-31]. It is observed from Fig 3 (b) that the XRD pattern of the PANI-SnO_2 nanocomposite exhibits the characteristic diffraction peaks of SnO_2 with 26.6% crystallinity and 73.4% amorphous nature due to PANI matrix. This indicates that the prepared nanocomposite sample of PANI-SnO_2 preserved crystalline nature of SnO_2 along with amorphous nature of PANI. This indicates that, as SnO_2 was dispersed in reaction mixer during polymerization of aniline, the formation of PANI matrix takes place on the surface of SnO_2 nanoparticles. This exhibits core-shell structure of nanocomposite of PANI metal oxide nanocomposite (PANI-SnO_2), which is also analyzed by Transmission Electron Microscopic images. From Fig 3 (c), it is observed that, preferred orientation peak (110) [31-35] is attributed to presence of SnO_2 and hence it's crystal structure, do not get affected due to surface activation by CuO or no extra peaks in the XRD pattern of PANI-SnO_2 film were found, as it may be in very minute amount dispersed on the surface of film.

III (D) SURFACE MORPHOLOGY

The FESEM images of PANI-SnO_2 composite films of various concentrations of SnO_2 (0.5M, 0.25M, and 0.125M) are shown in Fig. 4 (a-c), while Fig. 4 (d-f) shows surface activation by CuO on dipping PANI-SnO_2 film with 0.25M concentration of SnO_2 in copper nitrate aqueous solution for 15 min, 30 min and 45 min. Many researchers showed that, SnO_2 nanoparticles exhibit a granular structure [28-33], while from Fig. 4 (a-f), it is observed that morphology of PANI-SnO_2 and CuO activated PANI-SnO_2 nanocomposite films are characterized by the presence of large globules. It is clearly visible that PANI gets deposited at the surface of SnO_2 and the secondary nucleation growth of PANI takes place on the already existing PANI. Thus, the results of XRD, FTIR, FESEM and TEM have provided clear evidence that polymerization of aniline has been successfully achieved on the surface of SnO_2 nanoparticles and leads to core-shell structure. Fig. 4 (a-c) shows the PANI-SnO_2 nanocomposite with agglomeration. Also, from Fig. 4 (a-c), it is observed that, as the SnO_2 concentration increases, the particle size is also increases. The average particle size was found to be of ~ 6.8 nm. It is observed that the average grain size measured by XRD and SEM were not matching. This may happened due to the fact that two or more crystallites may be fused together to form a particle and cannot be resolved by SEM profile, but XRD can resolve the particles easily [34]. The growth of nanoparticles and further aggregate formation of material may be followed by diffusion limited cluster aggregation type mechanism instead of reaction limited cluster aggregation mechanism. According to P. Sandkuhler et al [35], diffusion limited cluster aggregation type mechanism, every collision

International Journal of Engineering Research & Technology (IJERT)
ISSN: 2278-0181
Vol. 5 Issue 10, October-2016

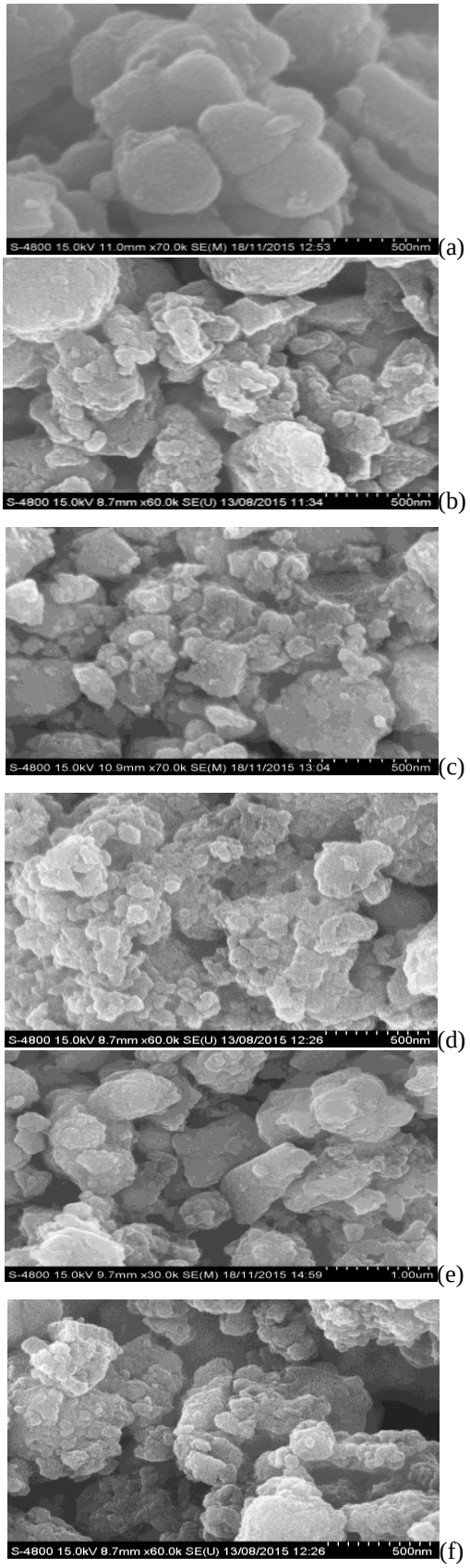

Fig. 4: FESEM images of PANI SnO_2 (a)0.5M, (b)0.25M, (c) 0.125M and CuO activated PANI-SnO_2 (d) 15 min, (e) 30 min and (f) 45 min.

between two clusters results in the formation of a new cluster, followed by further aggregate formation. While in reaction limited cluster aggregation type mechanism, only a small fraction of all the collisions leads to the formation of new cluster. The SEM images support such growth of PANI-SnO_2 nanoparticles and further aggregate formation as a result of diffusion limited cluster aggregation mechanism. The surface activation of PANI-SnO_2 (with0.25M SnO_2) thick film by dipping in copper nitrate solution for 15 min. provides favorable surface morphology for gas response which leads to maximum ammonia response at room temperature.

III (E) EDAX ANALYSIS

The chemical composition analysis of PANI-SnO_2 thick films was performed by the energy dispersive analysis by X-ray (EDAX). The EDAX analysis exhibits prominent peaks of Sn and O with C, N, O, etc. as organic counter part of aniline. No additional peaks are detected indicating that prepared samples are free from impurities that arise from starting precursors. The mass % of Sn and O varies with varying concentration of SnO_2 in the reaction mixture.

III (F) TRANSMISSION ELECTRON MICROSCOPY

Fig. 5 (a) shows TEM micrograph of PANI-SnO_2 as prepared powder sample.

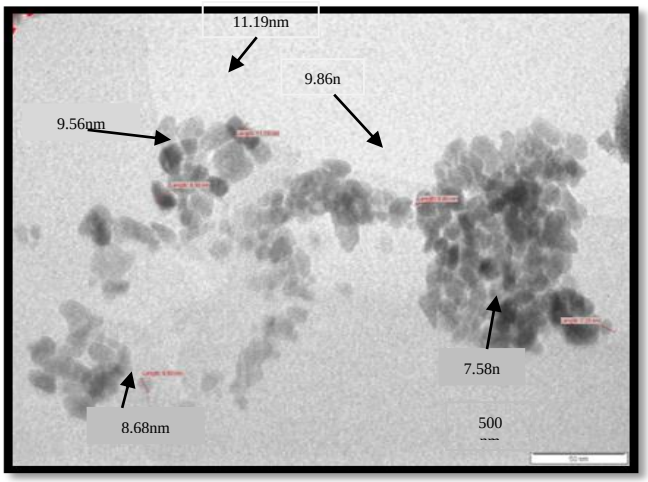

Fig. 5 (a): Transmission Electron Micrograph of PANI-SnO_2 (0.25M)

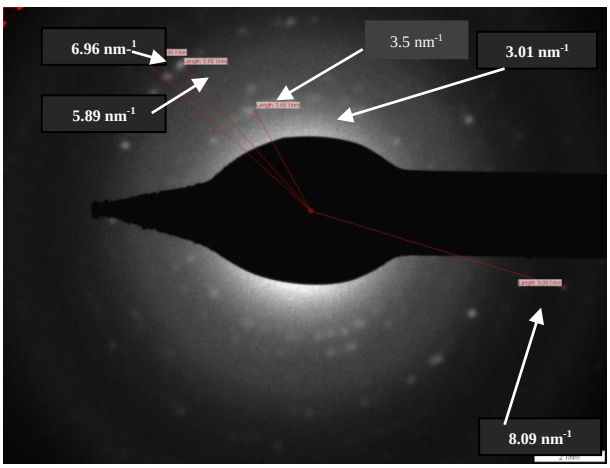

Fig. 5 (b): Diffraction pattern of PANI-SnO_2 (0.25M)

It supports core shell spherical nanocrystal structure. The average particle size was found to be of ~ 9.37nm. The crystallite size observed by TEM is in good agreement with the value determined by SEM (~6.8 nm). The electron diffraction

International Journal of Engineering Research & Technology (IJERT)
ISSN: 2278-0181
Vol. 5 Issue 10, October-2016

pattern of PANI-SnO_2 in Fig. 5 (b) exhibits concentric rings made up of discrete spots indicating the nano-sized polycrystalline nature of as prepared sample. The crystalline structure corresponding to planes (110), (101), (220), (112) and (321) are consistent with the peaks observed in the XRD pattern. XRD and TEM studies confirmed tetragonal structure of SnO_2. The diameter of each ring of diffraction pattern is measured as 3.01 nm^{-1}, 3.5 nm^{-1}, 5.89 nm^{-1}, 6.96 nm^{-1} and 8.09 nm^{-1}. The reciprocal of these values give the inter-planar distance d values. In table 1, d values from XRD and diffraction pattern of TEM are summarized.

XRD d values (A^0)	Electron diffraction (TEM)		Plane (hkl)
	Reciprocal of d values δ_{hkl} (nm^{-1})	d values (A^0)	
3.351	3.01	3.32	110
2.644	3.5	2.8	101
1.75	5.89	1.69	220
1.439	6.96	1.436	112
1.215	8.09	1.236	321

Table 1: d values obtained from XRD and TEM

III (G) ELECTRICAL BEHAVIOR OF THE SENSOR

Fig. 6 depicts I-V characteristics of PANI SnO_2 composites with various concentrations of SnO_2. It exhibits the resistive or ohmic nature. PANI-SnO_2 (0.25 M) sample shows maximum conductivity (Fig. 7). The increase in conductivity may be attributed to the increase of charge transformation due increased surface: volume ratio, as shown in Fig. 4 (b) and may be due to reduced particle size as evidence by TEM image as shown in Fig. 5. It has been observed that, the conductivity of the samples increases with the operating temperature, showing negative temperature coefficient of resistance (NTC). Thus, the samples represent semiconducting nature. The increase in conductivity is due to the increase in charge transfer by contribution of polaron and bipolaron bands formation within wide band gap of composites between SnO_2 and PANI chain with increase in temperature [36].

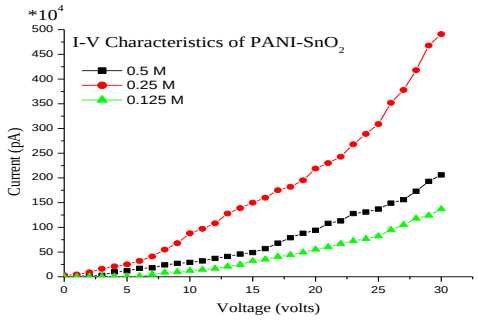

Fig. 6: I-V characteristics of PANI SnO_2

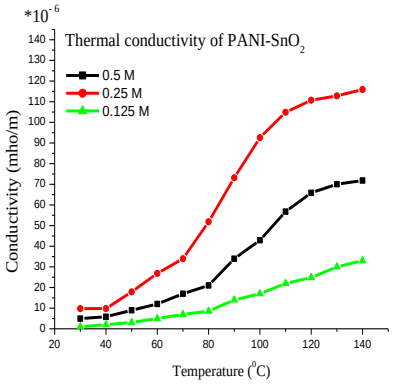

Fig. 7: Thermal characteristics of PANI SnO_2

IV GAS SENSING PERFORMANCE OF THE SENSOR

IV (A) EFFECT OF OPERATING TEMPERATURE

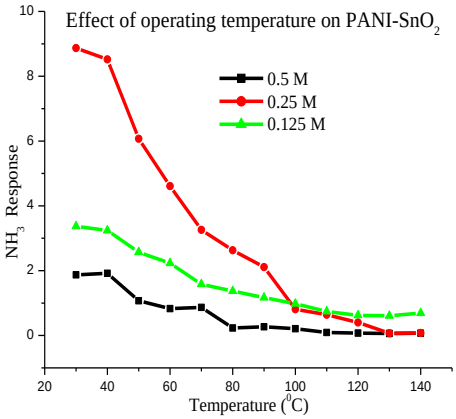

Fig. 8 (a): NH_3 response vs. operating temperature of PANI-SnO_2 (0.25M)

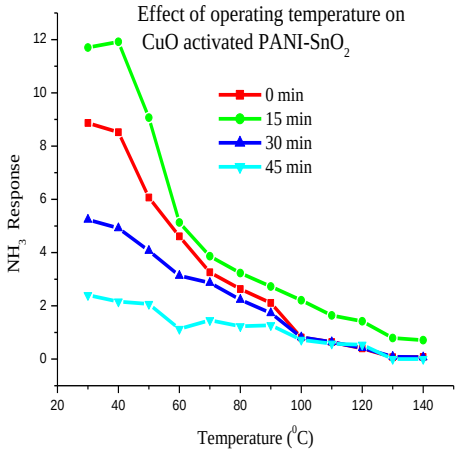

Fig. 8 (b): NH_3 response vs. operating temperature of CuO activated (15 min) PANI-SnO_2(0.25M)

All adsorption, desorption and diffusion processes are temperature dependent, which are responsible for gas sensing mechanism of the sensor. It was observed from Fig. 8 that, gas response varies with change in operating temperature. Fig. 8 (a) shows variation of NH_3 response against operating temperature

International Journal of Engineering Research & Technology (IJERT)
ISSN: 2278-0181
Vol. 5 Issue 10, October-2016

for different samples of PANI-SnO_2 with varying concentration of SnO_2, viz. 0.5M, 0.25M and 0.125M. The sensor with 0.25M concentration of SnO_2 incorporated in PANI matrix shows maximum response of 8.8 to ammonia gas at room temperature, among all. This sensor also shows considerable response (5.7) to ethanol, (2.2) to chlorine and (1.7) to CO_2 gas at room temperature.

All of these sensors show maximum response to NH_3 but suffering from poor selectivity (Fig. 10) against other gases, LPG, Ethanol, CO_2, H_2, Cl_2 and H_2S. The sensor was then surface activated by dipping it in to 0.01M copper nitrate solution for different intervals of time viz. 15 min, 30 min and 45 min. Fig. 8 (b) shows the variation of NH_3 gas response with operating temperature for CuO activated PANI-SnO_2 samples for different dipping time. Out of these, the sensor activated for 15 min shows maximum response of 11.7 to NH_3 gas at room temperature.

IV (B) ACTIVE REGION OF THE SENSOR

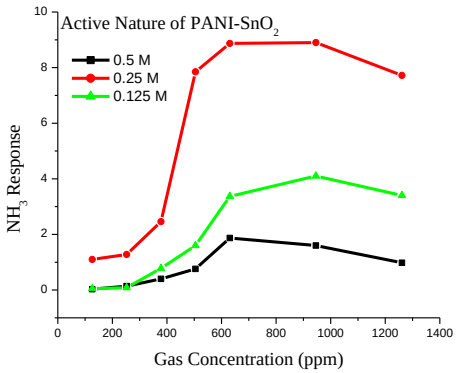

Fig. 9 (a): Variation in response with NH_3 gas concentration in ppm for PANI-SnO_2

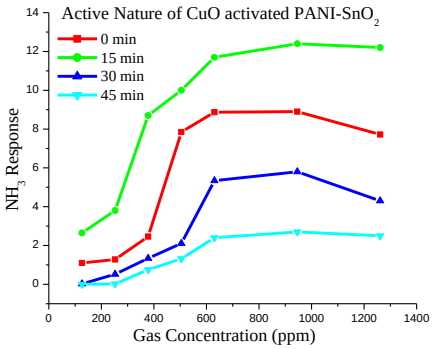

Fig. 9 (b): Variation in response with NH_3 gas concentration in ppm for CuO activated PANI-SnO_2

When the PANI-SnO_2 thick film was exposed to varying concentration of NH_3, the gas response observed to increase continuously with increasing concentration of NH_3 at optimum temperature. Fig. 9 (a) shows variation of NH_3 gas response with ammonia gas concentration in ppm, for the sensor composite of PANI-SnO_2 at room temperature. Fig. 9 (b) shows variation of NH_3 response with ammonia gas concentration for CuO activated PANI-SnO_2 samples for 15 min., 30 min. and 45 min. dipping time. All the samples show initial rapid increase in gas response from 20 to 50 ppm and then saturates beyond 50 ppm. Thus active region for these samples is 20 ppm to 50 ppm. However, in case of CuO activated PANI-SnO_2 samples respond to NH_3 at 10 ppm. Thus the active region for these samples is from 10 ppm to 50 ppm of NH_3 at room temperature. It indicates that surface activation of PANI-SnO_2 with CuO (for 15 min dipping time) improves the active nature region. Exposure to large concentration of gas form multilayer of gas molecules on film surface, due to multilayers, gas molecules remain there as inactive molecules which slows down the rate of increase of gas response.

IV (C) SELECTIVITY OF THE SENSOR

Fig. 10 (a) depicts the selective nature of the PANI–SnO_2 sensor for 20 ppm NH_3 against various gases at room temperature. PANI–SnO_2 (0.25M) sensor shows maximum response to NH3 among all. However, it suffers from poor selectivity against ethanol and Cl_2 gases. It was observed in Fig. 10 (b) that, CuO activated PANI–SnO_2 (0.25M) for 15 min enhanced the response to NH_3 at room temperature. The same sample exhibits the considerable response to LPG and CO_2 among all other gases viz. LPG, NH_3, CO_2, Ethanol, H_2, Cl_2, and H_2S. Also, it was observed from Fig. 10 (b) that, after CuO activation for 15 min, PANI–SnO_2 (0.25M) sample enhances the LPG response than without activated film.

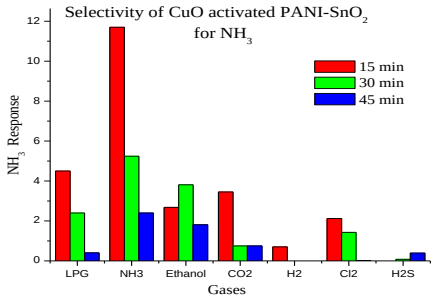

Fig. 10 (a): Selective nature of PANI-SnO_2

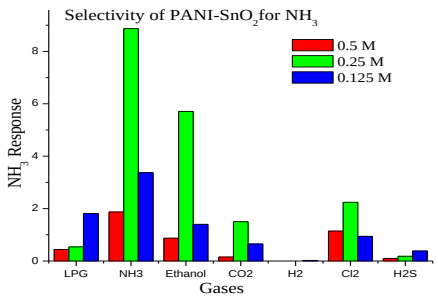

Fig. 10 (b): Selective nature of CuO activated PANI-SnO_2 for ammonia gas

International Journal of Engineering Research & Technology (IJERT)
ISSN: 2278-0181
Vol. 5 Issue 10, October-2016

IV (D) RESPONSE-RECOVERY PROFILE OF THE SENSOR

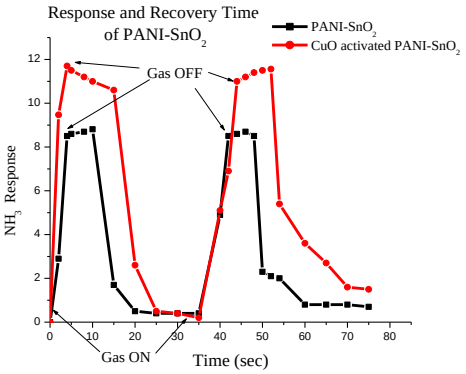

Fig.11: Response and recovery of the sensor

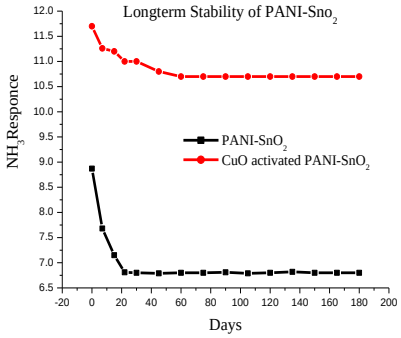

Fig.12: Long term stability of the sensor

Fig. 11 shows response and recovery time of PANI-SnO_2 sample with SnO_2 concentration of (0.25M) and CuO activated PANI-SnO_2 which is dipped in copper nitrate solution for 15 min. It was observed that, the sensor shows quick response (~4 s) to 20 ppm NH_3 and fast recovery (~15 s).

IV (E) LONG TERM STABILITY OF THE SENSOR

To ensure the reliability, important parameter of gas sensors is their stability over long duration. It reduces uncertainty in the results and improves the durability of sensor. Hence it is essential to pay attention towards long term stability of gas sensor. Mainly pure PANI is highly reactive and shows changes in oxidation states in open air atmosphere which leads to poor long term stability. Stability of the sensor films can be extended by doping PANI with inorganic elements, post processing treatments like annealing and capping sensor film surface with certain element. It is observed from Fig. 12 that, PANI-SnO_2 (0.25M) shows 23.34% decrease in the gas response within 150 days. However, CuO activated sample with dipping time of 15 min. shows 8.56% decrease within 60 days then after preferably remains constant.

IV (F) AMMONIA SENSING MECHANISM

The physical properties of conducting polymers strongly depend on their doping levels. Fortunately, the doping levels of conducting polymers can be easily changed by chemical reactions with many analytes at room temperature. This provides a simple technique to detect the analytes. Most of the conducting polymers are doped / undoped by redox reactions. Therefore, their doping level can be altered by transferring electrons from or to the analytes. Electron transferring can cause the changes in resistance and work function of the sensing material. This process occurred when thick films of PANI are exposed with NH_3 and other redox-active gases. Electron acceptors can remove electrons from the aromatic rings of conducting polymers. When this occurs at a p-type conducting polymer, the doping level as well as the electric conductance of the conducting polymer is enhanced. An opposite process will occur when detecting an electron donating gas. Ammonia is an electron donor gas.

CONCLUSIONS

1. Pure PANI is insensitive to NH_3 gas even at higher gas concentration (1000 ppm).
2. Pure PANI can be loaded by post-transition metal oxide (SnO_2) as an additive, by the low cost technique.
3. Optimized mass% of CuO as an activator in PANI-SnO_2 enhances the NH_3 gas sensing performance of the sensor.
4. Among the various metal oxide additives tested, CuO activated SnO_2 loaded PANI is outstanding in promoting the NH_3 gas sensing performance of the material.

REFERENCES:

[1] L. A. Patil, D. R. Patil, Heterocontact type CuO-modified SnO_2 sensor for the detection of a ppm level H_2S gas at room temperature, Sens. Actuators B 120 (2006) 316-323.
[2] D. R. Patil, L. A. Patil, Room temperature chlorine gas sensing using surface modified ZnO thick film resistors, Sens. Actuators B 123 (2007) 546-553.
[3] D. R. Patil, L. A. Patil, D. P. Amalnerkar, Ethanol gas sensing properties of Al_2O_3-doped ZnO thick film resistors, Bulletin Mater. Sci.-Springer link 30 (2007) 553-559.
[4] S. D. Kapse, F. C. Raghuwanshi, V. D. Kapse, D. R. Patil, Characteristics of high sensitivity ethanol gas sensors based on nanostructured spinel $Zn_{1-x}Co_xAl_2O_4$, J. Current Appl. Phys. 12 (2012) 307 – 312.
[5] D. R. Patil, L. A. Patil, Preparation and study of NH_3 gas sensing behavior of Fe_2O_3 doped ZnO thick film resistors, Sens. Transducers 70 (2006) 661-670.
[6] D. R. Patil, L. A. Patil, P. P. Patil, Cr_2O_3-activated ZnO thick film resistors for ammonia gas sensing operable at room temperature, Sens. Actuators B 126 (2007) 368–374.
[7] D. R. Patil, L. A. Patil, Ammonia sensing resistors based on Fe_2O_3-modified ZnO thick films, Sensors IEEE 7 (2007) 434-439.
[8] U. B. Gawas, V. M. S. Verenkar, D. R. Patil, Nanostructured ferrite based electronic nose sensitive to ammonia at room temperature, Sens. Transducers 134 (2011) 45-55.
[9] K. A. Khamkar, S. V. Bangale, V. V. Dhapte, D. R. Patil, S. R. Bamne, A Novel Combustion Route for the Preparation of Nanocrystalline $LaAlO_3$ Oxide Based Electronic Nose Sensitive to NH_3 at Room Temperature, Sens. Transducers 146 (2012) pp. 145-155.
[10] M. S. Shinde, D. R. Patil, R. S. Patil, Ammonia gas sensing property of nonocrystalline Cu_2S thin films, I. J. Pure and Applied Physics, 51, (2013) pp 713-716.
[11] http://www.nobel.se
[12] H. Shirakawa, E. J. Louis, A. G. MacDiarmid, C. K. Chiang, A. J. Heeger, Chem. Commun. 578 (1977).
[13] T. A. Skotheim, R. L. Elsenbaumer, J. R. Reynold (eds), Hand book of conducting polymer, 2nd ed., Dekker, New York 1998.
[14] M.OzDen, E. Ekinci, A. E. Koragozlor; Electrochemical preparation and sensor properties of conducting PANI films; Trurk Journal of Chemistry 23(199) 89 – 98.
[15] Zakrzewska K. Mixed Oxides as gas sensors; Thin Solid Films 391 (2001)
[16] Dubbe A, Fundamentals of solid State ionic micro gas sensors; Sensors and Actuators: B 88 (2003)138 – 148.
[17] S.S.Joshi, C.D. Lokhande, Sung – Hwan Han; A room temperature liquefied petroleum gas sensor based on all electrodeposited n-CdSe/p-PANI junction; Sensors and Actuators: B 123 (2007) 240 – 245.

International Journal of Engineering Research & Technology (IJERT)
ISSN: 2278-0181
Vol. 5 Issue 10, October-2016

[18] N. G. Deshpande, Y. G. Gudage, Ramphal Sharma, J. C. Vyas, J.B. Kim, Y. P. Lee; Studies on tin oxide – intercalated PANI nanocomposite for ammonia gas sensing applications; Sensors and Actuators; B 138 (2009) 76 – 84.
[19] Narsimha Prvatikar, Shilpa Jain Syed Khasim M Revansiddappa, S. V. Bhoraskar M.V.N. Ambika Prasad; Electrical and humidity sensing properties of PANI/WO_3 composites, Sensors and Actuators; B 114 (2006)
[20] Anjali A. Athavale, Milind V. Kulkarni; PANI and its substituted derivatives as sensors for aliphatic alcohols; Sensors and Actuators; B 114 (2007)
[21] Subhash B.Kondawar, S. P. Agrawal, S.H. Nimkar P. T. Patil; Conductive PANI-tin nanocomposites for ammonia sensor; Adv. Mat. Letters, 3(5) (2012),pp 393-398.
[22] S. B. Kondawar, S. P. Agrawal, S.H. Nimkar, H. j. Sharma, P. T. Patil; Conductive PANI=tin oxide nanocomposites for ammonia sensor; Adv. Mat.Lett. 3(5), (2012) pp 393-398.
[23] D. S. Dhawale, D.P. Dubal, A. M. More T, P. Gujar, C. D. Lokhande; Room temperature liquefied petroleum gas (LPG)sensor; Sensors and Actuators; B 147 (2010) 488 – 494.
[24] D. S. Dhawale, D.P. Dubal, V. S. Jamadade, R. P. Salunkhe, S. S. Joshi, C. D. Lokhande; Room temperature LPG sensor based on n-CdS/p-PANI heterojunction; Sensors and Actuators; B 145 (2010) 205 – 210.
[25] L. A. Patil, J. P. Talegaonkar; Synthesis of WO_3 – PANI composite and their gas sensing properties; Sensors and Transducers 113(2) (2010) 82 – 94.
[26] Satish Sharma Chetan Nikhare, Sushama Pethkar, Anjali Athawale; Chloroform vapour sensor based on copper/PANI nanocomposite; Sensors and Transducers 85 (2002) 131 – 136.
[27] N.G. Deshpande, Y. G. Gudage, Ramphal Sharma, J.C. Vyas, J.B. Kim, Y.P. Lee; Studies on tin oxide-intercalated PANI nanocomposite for ammonia gas sensing application; Sens and Actu. B 138(2009) pp 76-84.
[28] Shuang Zhan, Dongmei Li, Shengfa Liang, Xin Chen and Xia Li; A Novel Flexible Room Temp. Ethanol Gas Sensor Based on SnO2 doped Poly-Diallylimethylammonium Choride; Sensors, doi: 10.3390/s 130404378; 13 (2013) pp 4378 – 7389.
[29] Sbel Gurakar, Tulay Serin, Necmi Serin; Electrical and microstructural properties of (Cu, Al, In)-doped SnO_2 films deposited by spray pyrolysis; Adv. Mat. Lett. 5(6), (2014) pp 309-314.
[30] Ayeshamariam, R. Perumal Samy; Synthesis, Structural and optical Characterization of SnO_2; J. on Photonics and spintronics; 2, 2(2013) ISSN234-8572 (print).
[31] O. Alizadeh Sahraei, A. Khodadadi, Y. Mortazavi, M. Vesali Naseh and S. Mosadegh; World Academy of Sci. Engg. And Techn.49 (2009) pp 185-188.
[32] D. R. Patil, Ph. D. Thesis (2007) North Maharashtra University, Jalgaon.
[33] D. S. Sutrave, G. S. Shahane, V. B. Patil, L. P. Deshmukh; Micro-crystallographic and optical studies on $Cd_{1-x}Zn_xSe$ thin films ; Mat. Chem Phy.; 65(2000) pp 298-305 films
[34] P. Sandkuhler J. Sefcik, M. Morbidelli, Kinetics of gel formation in dilute dispersion with strong attractive particle interactions; Adv. Colloid Interf. Sci. 108/ 109 (2004) pp 134-143.
[35] Subhash B. Kondawar, Pallavi T. Patil, Shikha P. Patil, chemical vapor sensing properties of electrospun nanofibers of PANI / ZnO nanocomposite, Adv. Mat. Letters 5 (7) (2014) pp 389-395.